Sancho-Parramon, Jordi; Jelovina, Denis. Boosting Fano resonances in single layered concentric core–shell particles. // Nanoscale. 6 (2014); 22, 13555-13564 (postprint version)

Boosting Fano resonances in single layer concentric core-shell particles

Jordi Sancho-Parramon,[*a] **and Denis Jelovina**[b]

Efficient excitation of Fano resonances in plasmonic systems usually requires complex nano-structure geometries and some degree of symmetry breaking. However, a single-layer concentric core-shell particle presents inherent Fano profiles in the scattering spectra when sphere and cavity modes spectrally overlap. Weak hybridization and proper choice of core and shell materials gives place to strong electric dipolar Fano resonances in these systems and retardation effects can result in resonances of higher multipolar order or of magnetic type. Furthermore, proper tailoring of illumination conditions leads to an enhancement of the Fano resonance by quenching of unwanted electromagnetic modes. Overall, it is shown that single layer core-shell particles can act as robust Fano resonators.

1 Introduction

The Fano resonance (FR) is a characteristic signature of quantum systems resulting from the interference of a broad spectral continuum and a narrow discrete state [1]. During the last years, classical analogies of FR have been observed in plasmonic nano-structures [2,3], where bright and dark plasmon modes play the role of continuum and discrete states, respectively. The bright plasmon resonance can be directly excited by the incoming radiation and also by its electromagnetic coupling to the dark mode. The interference between these two excitation pathways gives place to FR in the radiated light spectra [4]. Strictly speaking, the plasmon mode acting as discrete state does not have to be completely dark, i.e., interference between super-radiant and sub-radiant plasmon resonances can also results in FR [3,5,6]. Overall, the FR in plasmonic systems is interesting due to its asymmetric line-shape, strong dispersion and scattering suppression. These characteristics may lead to multiple applications such as plasmonic rulers [7,8], sensing [9–11], cloaking [12], fluorescence enhancement [13], optical switching [14] and optical manipulation [15] .

The efficient excitation of FR in plasmonic systems requires spectral overlapping and strong interaction of the involved plasmon modes [4]. In this sense, plasmonic oligomers are excellent candidates for FR generation since the complex mode hybridization that takes place through near field coupling of closely located particles enables largely tunable mode engineering [16–19]. The characteristics of FR in oligomers are highly dependent on the environment, making them very suitable for sensing applications [16,20]. However, the FR is also strongly sensitive to the oligomer geometry and highly accurate fabrication techniques such as electron beam lithography are required to avoid variations from the targeted resonance frequency and line-shape. In addition, most of up-to-date fabricated plasmonic oligomers are planar structures, having intrinsically anisotropic electromagnetic behaviour and only certain symmetric configurations can lead to polarization-independent response for a given propagation direction [21,22]. An alternative widely studied structure for generation of plasmonic FR are core-shell single particles, that have isotropic optical response and can be synthesized by large-throughput and cost-efficient chemical methods. The electromagnetic response of core-shell particles has been largely investigated since this system enables achieving total scattering cancellation and hence represents a canonical example of cloacking device [23].. Multi-layered core-shell particles can give place to FR arising from the interaction between hybridized modes that result from the coupling of plasmons excited at different metal-dielectric interfaces [24–26]. Additional FR can be also observed in non-concentric core-shell particles [24,27–29], since symmetry breaking induces electromagnetic coupling between otherwise non-interacting orthogonal modes [30]. However, FR can take place even in single-layer concentric core-shell particles. For instance, bimetallic particles present FR as result of the interaction between narrow plasmon modes and broad core interband transitions [31], in analogy with the case of metallic heterodimers [32]. FR have been also observed in silver-core dielectric-shell particles [33] and explained in terms of the interference between light scattered by the plasmon mode and the dielectric shell. More generally, FR have been theoretically predicted for plasmonic-core dielectric-shell particles. [34] Finally, in the context of scattering cancellation it has been pointed out that, in the dipolar approximation, coupling between hybridized bonding and anti-bonding modes in dielectric-core metal-shell small particles can give place to FR [28,35]. This type of FR can be further modulated if a radially anisotropic core is considered. [36] As a general rule, there is a correlation between structure complexity and FR excitation efficiency and consequently the FR in a single-layer concentric core-shell geometry is significantly weaker than those

[0a] *Rudjer Boskovic Institute, Bijenicka cesta 54, Zagreb 10000, Croatia. E-mail: jsancho@irb.hr*

[0b] *Chemistry Department, Faculty of Sciences, Universidad Autónoma de Madrid, Ciudad Universitaria de Cantoblanco, 28049 Madrid, Spain.*

observed in multilayered asymmetric particles or in plasmonic oligomers.

In the present study we numerically investigate how a proper choice of material properties, geometry and illumination conditions may lead to strong FR in single-layer concentric core-shell particles in the optical range. The key issue is weak hybridization between cavity and sphere modes. In this regime, a proper choice of core and shell properties can result into FR of electric dipolar nature and, when retardation effects become significant, of higher multipolar order and even of magnetic type. Generation of FR is shown in metal-dielectric, dielectric-metal and all-dielectric core-shell particles. Furthermore, controlling the intensity and polarization distribution of light enables selective mode excitation and FR enhancement. The present results indicate that properly designed and excited single layer core-shell particles, that can be fabricated with well-established techniques, behave as effective and robust systems for FR generation.

2 Numerical methods

Exact calculation the electromagnetic response of a core-shell particle can be performed analytically using the extension of Mie theory[37] developed by Aden and Kerker[38]. Basically, all the involved fields (incident, scattered and the fields in the shell and in the core) are expanded in vector spherical harmonics that represent multipole electric and magnetic fields. Imposing boundary conditions at the interfaces of the particle (core-shell and shell-external medium) the expansion coefficients can be determined. Then the extinction and scattering cross sections, defined as the ratio between extinguished and scattered energy rates and the incident irradiance, can be calculated as $C_{ext} = \frac{2\pi}{k^2}\sum_{n=1}^{N}(2n+1)\,Re\,(a_n+b_n)$ and $C_{sca} = \frac{2\pi}{k^2}\sum_{n=1}^{N}(2n+1)\left(|a_n|^2+|b_n|^2\right)$ where a_n and b_n are the scattered field expansion coefficients for the electric and magnetic multipoles of order n, N is the largest multipole order considered and k is the wave-number in the incident medium. One should note that the scattering associated with each multipolar order adds incoherently to the total scattering cross section. The absorption cross section can be computed as $C_{abs} = C_{ext} - C_{scatt}$. Dimensionless extinction (Q_{ext}), scattering (Q_{scatt}) and absorption (Q_{abs}) efficiencies are obtained dividing the corresponding cross sections by the cross sectional area of the particle (πr_s^2) , being r_s the shell radius. In all the calculations, the number of multipoles N has been increased till convergence of the computed quantity was achieved in all the range of interest where parameters (photon energy, dielectric function, particle sizes) were varied. Typically, N is larger for near-field quantities than for cross sections[39].

In the original work of Aden and Kerker the considered incident field was a plane wave. In the present work we consider also other illuminations schemes that can be implemented in the same calculation scheme by expanding the incident field in vector spherical harmonics. Thus, a focused plane wave can be treated with the multipolar expansion developed by Sheppard and Török,[40] that has been used to study the influence of tight focusing on the plasmon spectra of single particles[41] and particle dimers[39]. As the degree of focusing increases, the relative weight of high order vector spherical harmonics decreases[40,41]. In addition, we also consider illumination by cylindrical vector beams. In this case, we use the field expansion provided by Borghi et al.[42]. This study shows that the expansion of radially (azimuthally) polarized focused beams requires the use of vector spherical harmonic representing only electric (magnetic) multipoles[43,44]. Generally speaking, the expansion of an arbitrary field distribution into vector spherical harmonics can be computed numerically[37]. We use this approach to calculate the response of particles illuminated by focused Hermite-Gaussian beams.

The cross sections and efficiencies defined for plane wave excitation loose their meaning if other illumination schemes are considered. Thus, for the focused plane waves, Hermite-Gaussian beams and cylindrical vector beams cases studied in the present work we have used normalized efficiencies. They are defined as the ratio between the power extinguished and scattered by the particle and the average incident power crossing the particle cross section at the focal plane and divided by the cross sectional area of the particle. For a weakly focused plane wave this quantity trends to the efficiency value of a plane wave. For cylindrical vector beam, the power crossing the focal plane vanishes at the optical axis where the particle is located and a quantitative interpretation of the normalized efficiencies may be inappropriate for comparison with plane waves[43].

3 Results and discussion

3.1 Composition and size effects

We start our analysis by revisiting the optical properties of metal-shell dielectric-core nanoparticles[45–48]. In the quasi-static limit, the largely tunable electromagnetic response of these particles can be understood in terms of the hybridization between sphere (ω_s) and cavity (ω_c) modes, corresponding to dipole plasmons excited at the shell-external medium and core-shell interfaces, respectively (Fig. 1.a)[49]. The interaction between these modes results in a super-radiant bonding (ω_b) and a sub-radiant anti-bonding (ω_a) resonance that split away as mode coupling increases, i.e., as the core-to-shell radius ratio is reduced, in a similar fashion as it happens with odd and even surface plamon polaritons in thin metal films[50,51]. Since super-radiance implies spectrally broad resonances[52], the bonding and anti-bonding modes can act as the continuum and discrete

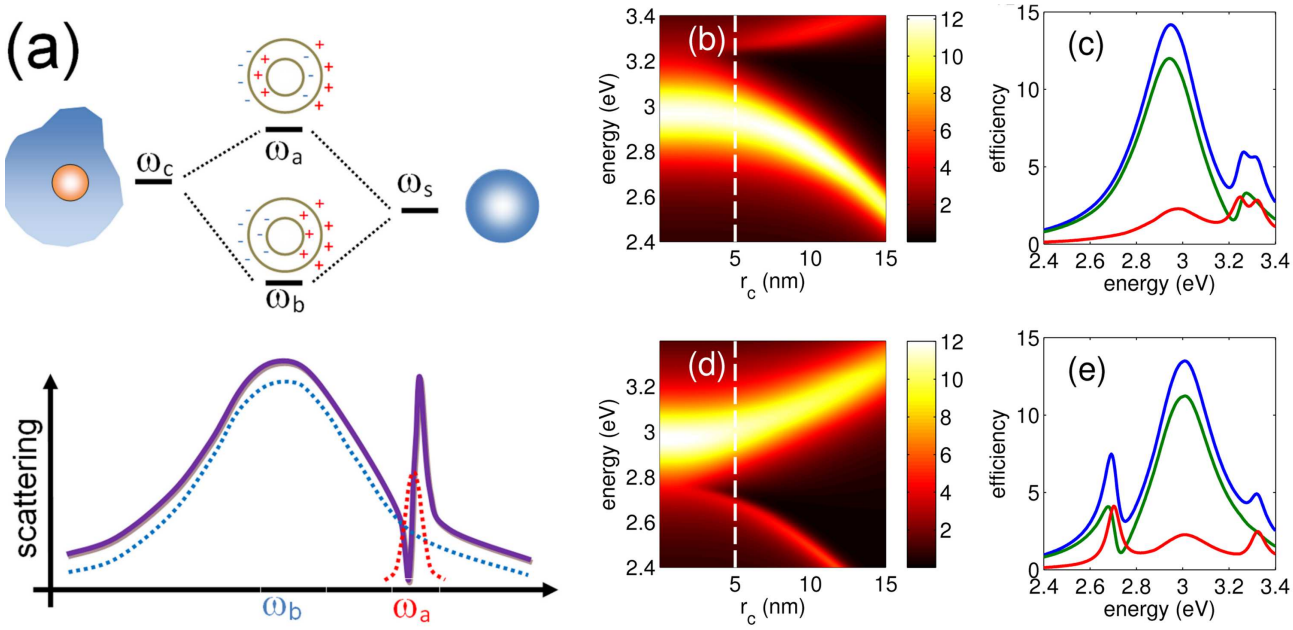

Figure 1 Scheme of hybridization of plasmon modes in a core-shell nanoparticle and generation of FR due to the overlapping of bonding (ω_b) and anti-bonding (ω_a) modes (a). Scattering efficiency spectra for a silver-shell dielectric-core particle embedded in water with $r_s = 30$ nm for $\varepsilon_c = 7$ (b) and for $\varepsilon_c = 14$ (d). Extinction (blue), scattering (green) and absorption (red) efficiencies for $\varepsilon_c = 7$ (c) and for $\varepsilon_c = 14$ (e) when $r_c = 5$ nm.

state necessary to generate a Fano line-shape in the scattering spectra.

In order to illustrate the appearance of FR in these systems, we calculate the optical response of a silver-shell dielectric-core particle. In Fig.1.b it is shown the scattering efficiency spectra (Q_{scatt}) for such particle, using the data of Johnson and Christy for silver[53] and setting the dielectric function of the core to $\varepsilon_c = 7$. The shell radius is $r_s = 30$ nm and the core radius, r_c, is varied from zero to $r_s/2$. The particle is assumed to be in a water-like environment with dielectric function $\varepsilon_m = 1.77$, same as for the rest of simulations except otherwise stated. For small r_c values hybridization is weak and the two observed resonances essentially correspond to the primitive modes, i.e., the anti-boding resonance is a cavity-like mode that takes place at the photon energy where the Frölich condition $\varepsilon_c = -2\varepsilon_s$ is fulfilled, where ε_s is the shell dielectric function. The bonding resonance is a sphere-like mode that occurs at an energy given by the size-corrected Frölich condition[37], $\varepsilon_s = -(2 + 12x_s^2/5)\varepsilon_m$ with x_s being the size parameter of the shell. FR can be clearly observed in this weak hybridization regime, as shown in Fig. 1.c for a particle with $r_c = 5$ nm: the excitation of the anti-bonding mode in the absorption efficiency (Q_{abs}) at 3.2 eV coincides with the FR line-shape in the scattering spectrum. As the value of r_c increases, the anti-bonding and bonding mode shift to higher and lower energies respectively and the spectral overlapping of the modes, and hence the FR strength, reduces.

In order to quantify this effect and estimate the strength of the FR we have fitted the scattering spectra to the analytical model based on the interaction of electromagnetic modes recently proposed by Gallinet and Martin.[54,55] (see Supporting Information). In this model, the FR line-shape is characterized by two parameters: b, the modulation damping parameter that originates from absorption losses and q, the asymmetry parameter defined as the ratio between the optical response of the sub-radiant mode and the continuum. As hybridization increases, both $|q|$ and b become larger, asymmetry is damped and the scattering line-shape for energies around the sub-radiant mode becomes Lorentzian-like. Qualitatively, this is a similar situation to the one observed for FR in quadrumers[55]: when the interparticle separation decreases and electromagnetic coupling among particles increases, both $|q|$ and b become larger and the FR looses its characteristic line-shape. One should note, however, that the FR is not efficiently excited for very small r_c values. In this case, electromagnetic coupling is too weak compared to absorption losses and the resonance vanishes, i.e., the value of b increases, in analogy to the behaviour reported for dolmen plasmonic structures[55,56].

The case of a particle having a dielectric core with ε_c = 14 is shown in Fig. 1.d. For such particle the cavity mode is located at lower energy than the sphere mode and the sub-radiant anti-bonding and super-radiant bonding modes shift re-

spectively to lower and higher energies as the core-to-shell ratio increases[47,48]. Again, in the weak hybridization regime a FR can be clearly observed, as shown in Fig. 1.e. for the $r_c = 5$ nm case. As hybridization becomes stronger, the values of $|q|$ and b become larger and the FR vanishes (Supporting Information). It can be noted that now the sub-radiant mode is located at the low energy side of the super-radiant mode, hence resulting in an asymmetry Fano parameter $q < 0$[55], as opposite to the case with $\varepsilon_c = 7$, where $q > 0$.

The observed FR in the previous example are relatively weak compared to those that can be obtained in other plasmonic systems. Nevertheless, in the weak hybridization regime the FR located at lower energies ($\varepsilon_c = 14$) appears to be stronger than the one that takes place at higher energies ($\varepsilon_c = 7$), what can be explained in terms of the reduced absorption losses and, thus, plasmon damping that occur as resonances red-shift. Such behaviour, that is a common characteristic of plasmon resonances[57] including cavity modes[58], is even more evident if one considers Au instead of Ag as shell material (Figure 2 in Supplementary Information). In that case, FR are strongly damped due to the large losses in gold and they are only evident when taking place at small photon energies, i.e., for very large values of ε_c. The observed trend can be also verified if one analyzes the response of larger particles. Fig. 2.a. shows the scattering efficiency for a silver-shell dielectric-core with $r_c = 20$ nm and $r_s = 70$ nm, i.e., the shell thickness is large enough to avoid significant hybridization but still comparable to the Ag skin-depth thus enabling excitation of the cavity mode at the core-shell interface. Due to the lack of mode hybridization, the bright bonding sphere-like mode acting as continuum is unaffected by the value of ε_c. However, increasing ε_c shifts the narrow anti-bonding cavity-like mode to the red, where losses are smaller and the FR becomes stronger. This red-shift can be further enhanced by retardation increasing the particle size, as it can be seen in Fig. 2.b that shows the scattering efficiency of a core-shell particle with $r_c = 80$ nm and $r_s = 130$ nm, i.e., with the same shell thickness as in Fig. 2.a. The FR excitation also benefits from retardation through broadening of the bonding sphere-like mode that acts as a less dispersive continuum. The strengthening of FR with the increase of particle size can be seen in Figs. 2.c and 2.d that show the efficiency spectra of core-shell particles with $\varepsilon_c = 9$. The cavity-like mode in the absorption spectra and the corresponding Fano profile in the scattering spectra that takes place at 2.8 eV for the particle with $r_s = 70$ nm become significantly narrower as the resonance red-shifts to 1.58 eV for the particle with $r_s = 130$ nm. Quenching the effect of absorption by using large particle sizes enables the efficient excitation of FR when gold is used as shell material, even with moderate values of ε_c (Figure 3 in Supplementary Information).

One can observe that additional FR appear in the scattering spectra as the particle size increases, corresponding to the exci-

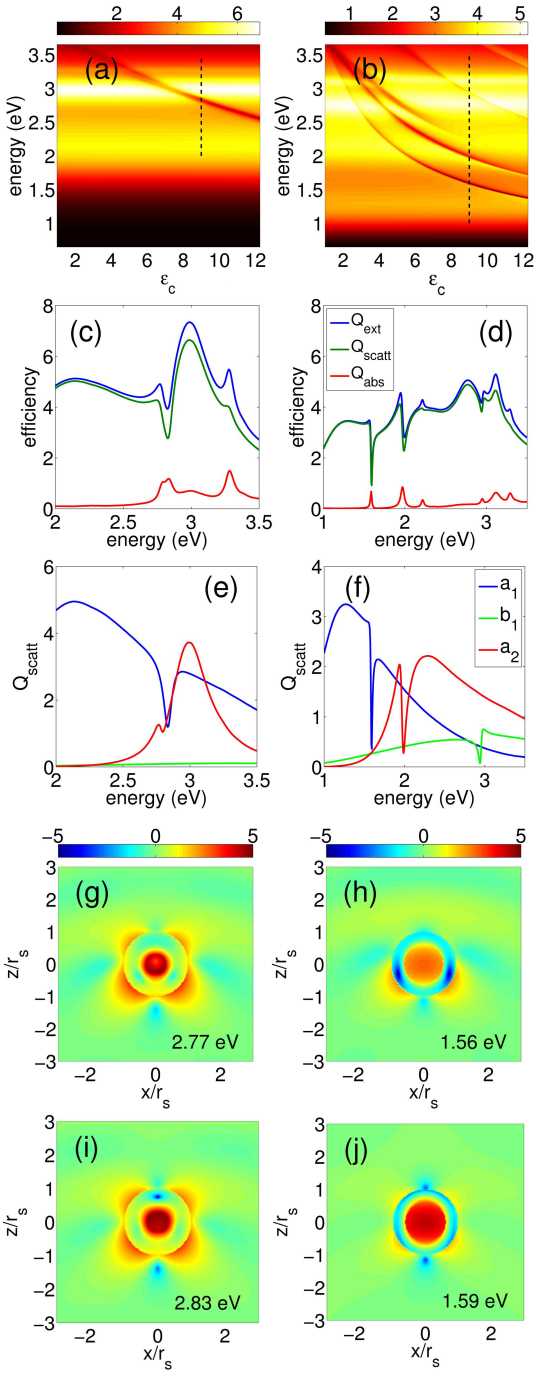

Figure 2 Scattering efficiency for a silver-shell dielectric-core particle (a, b). Extinction, scattering and absorption efficiencies for $\varepsilon_c = 9$ (c, d) and scattering contributions from different multipolar orders (e, f). Square amplitude (log scale) of the total electric field in the near field region for energies slightly below (g, h) and at the dip (i, j) of the dipolar FR. The incident field is x-polarized and propagates in the $z > 0$ direction. Left column (a, c, e, g, i) refer to particle with $r_c = 70$ nm and $r_s = 130$ nm and right column (b, d, f, h, j) to the particle with $r_c = 70$ nm and $r_s = 130$ nm.

tation of higher order sphere-like and cavity-like modes. As is the case for the dipolar FR, the excitation of a cavity-like mode in the absorption efficiency coincides with a Fano line-shape in the scattering spectra. Decomposing the scattering efficiency into its different multipolar contributions evidences this fact. Thus, for the $r_s = 70$ nm particle (Fig. 2.e) in addition to the electric dipolar FR (associated with the a_1 Mie scattering coefficient) there is also a closely located electric quadrupolar dip (a_2). In the $r_s = 130$ nm particle (Fig. 2.f), besides the electric dipolar, quadrupolar ($\approx$ 2 eV) and even octupolar ($\approx$ 2.2 eV) FR, a magnetic dipole FR (b_1) is also observed close to 3 eV. Likewise the dipolar FR, the higher order FR become more efficiently excited as they red-shift upon increase of particle size.

Although retardation induces strong FR by quenching the effect of losses, the higher order sphere-like plasmon resonances contribute with a background that does not interact with the cavity-like anti-bonding modes and thus ultimately limits the scattering cancellation at the Fano minimum[59]. The influence of the higher order resonances can be seen in the near field maps shown in Figs. 2.g to 2.j. In the particle with r_s = 70 nm there is a strong overlapping of the quadrupolar mode with the dipolar FR. As result, the near field distributions at a photon energy slightly below the FR (Fig. 2.g) and at the Fano dip (Fig. 2.i) are quite similar due to the significant quadrupolar contribution that masks the relatively weak modulation of the dipolar FR. For the particle with r_s = 130 nm, at photon energies below the dipolar FR (Fig. 2.h) the field distribution is basically of dipolar nature because there is weak overlapping with higher order modes. At the Fano dip (Fig. 2.h), however, the efficient cancellation between the dipoles of the cavity and shell leads to a near field map dominated by the quadrupolar contribution.

Fabrication of most of dielectric-core metal-shell particles is based on use of cores with relatively low dielectric constant such as SiO_2. In that case, the cavity mode is located at significantly larger energies than the sphere mode. In the non-retarded limit the cavity-mode falls into the range with large absorption losses, including inter-band transitions. Even if the particle size is increased and the resonances red-shift, the spectral overlapping between sphere-like and cavity-like modes remains insufficient for significant excitation of FR, as can be noticed from Figs. 2.a and 2.b. In the experimental works that have addressed the study of particles with large dielectric constant cores[47,48], the shell thickness was thin enough to lead to strong hybridization and avoid excitation of strong FR. These FR in the total scattering spectra have been also overlooked in theoretical studies on the optical properties of large dielectric constant core and metallic-shells that have focused either on the strong hybridization regime[60] or on off-resonance field enhancement and FR in directional scattering spectra[61]. The requirement of weak hybridization for the efficient excitation of FR indicates that, on the contrary to FR in oligomers, they are inadequate for sensing purposes because the FR position is almost uniquely determined by the cavity mode, i.e., by the core radius and the composing materials. Thus a more suitable application of these FR could be found in optical tagging[62] as their characteristic extinction and scattering line-shape is nearly independent of the medium where particles are located. In addition, the position, width and asymmetry of these FR would be unaffected by small variations of shell thickness during the fabrication process.

A metal-core dielectric-shell structure can also show Fano profiles in the scattering spectra that have been associated with the interference between the plasmon resonance of the metal core and the broad scattering background from the dielectric shell[33]. Figure 3 shows the scattering efficiency spectra for silver-core (r_c= 20 nm) SiO_2-shell particles embedded in a water-like medium. Even for a moderate value of the silica shell (r_s = 75 nm, Fig. 3.a.), the scattering efficiency shows the asymmetric profile characteristic of FR. The contributions of the plasmon mode of the core embedded in a silica environment and of a silica shell without the metal core are also displayed, indicating that the first acts as a narrow discrete mode with symmetric Lorentzian line-shape and the second as a broad continuum. For smaller shell sizes, the scattering from the shell is weaker and the Fano profile becomes Lorentzian-like. Hence, it was suggested that further enhancement of the FR could be achieved by providing larger scattering from the shell[33], i.e., by increasing the shell size factor as shown in Fig. 3.c., for a value of r_s = 150 nm. However, scattering from the shell starts displaying magnetic modes in addition to the dipolar electric Mie resonance when its size factor (i.e., thickness or refractive index) increases[63] (Fig.3.d). Thus, a larger shell size (Fig. 3.e) does not result in a significant enhancement of the Fano profile due to the magnetic and higher order electric modes (Fig. 3.f) that contribute to the total scattering efficiency but do not interact with the core electric dipolar plasmon mode.

In the previous cases the plasmon resonance plays an essential role on the excitation of FR by acting either as a discrete state (metal core) or broad continuum (metal shell). Plasmonic modes are also fundamental in the asymmetric line-shapes that have been observed in the scattering spectra of particles made of a metal core surrounded with a layer of J-aggregates[64]. This asymmetry that can be understood as result of the interaction of electric dipolar modes (plasmon and exciton) of significantly different width. In a broad sense, however, the basic requirement for FR excitation is that the mode associated with the shell and the one of the core have the same multipolar order and significant spectral overlapping. Thus, it could be possible to obtain similar FR as those described above for metal-core dielectric-shell particles by considering a large dielectric constant core that displays narrow Mie resonances[65]. Indeed, Mie resonances have been used for the excitation of FR in all-dielectric oligomers by combining the dipolar magnetic modes of silicon nanoparticles instead of the plasmon modes of metal

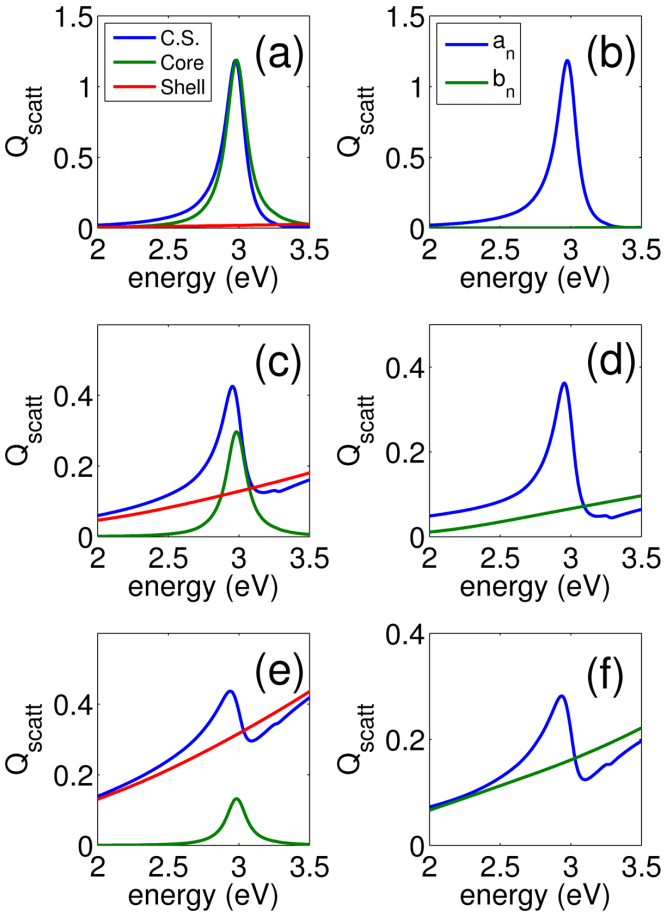

Figure 3 Scattering efficiencies of a 20 nm silver core surrounded by a silica shell of radius 75 (a), 150 (b) and 225 (c) nm (blue). The efficiency of a shell-only (red) and a core-only (green) particle is also shown. Right column shows the electric and magnetic contribution to the total scattering efficiency.

clusters[66,67]. Figure 4.a shows the scattering efficiency of a dielectric core (r_c = 100 nm) surrounded by a SiO_2 shell (r_s = 500 nm). The broad scattering band independent of ε_c is associated with the shell contribution while the superimposed narrow peaks are connected to Mie resonances from the core. The interaction of these narrow modes with the background provided by the shell gives place to several FR for large values of the core dielectric constant. Each of these FR corresponds to a different multipolar order, as can be seen from the multiple contributions to the scattering spectrum of a core with ε_c = 36 (Fig. 4.b). One can notice that in absence of absorption the scattering cancellation is complete for a FR of given order and the value of total scattering at the dip value is limited by the contribution of other multipolar orders. The large values of the dielectric function necessary to obtain narrow FR are not accessible in naturally available materials in the optical range. For instance, silicon or germanium have $\varepsilon_c \approx 16$ and their Mie resonances have a width comparable to the shell modes. However, the effective dielectric function of composite plasmonic materials consisting of densely packed metal nanoparticles can show large values for energies below the plasmon resonance as it has been theoretically predicted[68] and experimentally demonstrated[69]. These artificial dielectric composites may pave the path towards all-dielectric FR in core-shell systems.

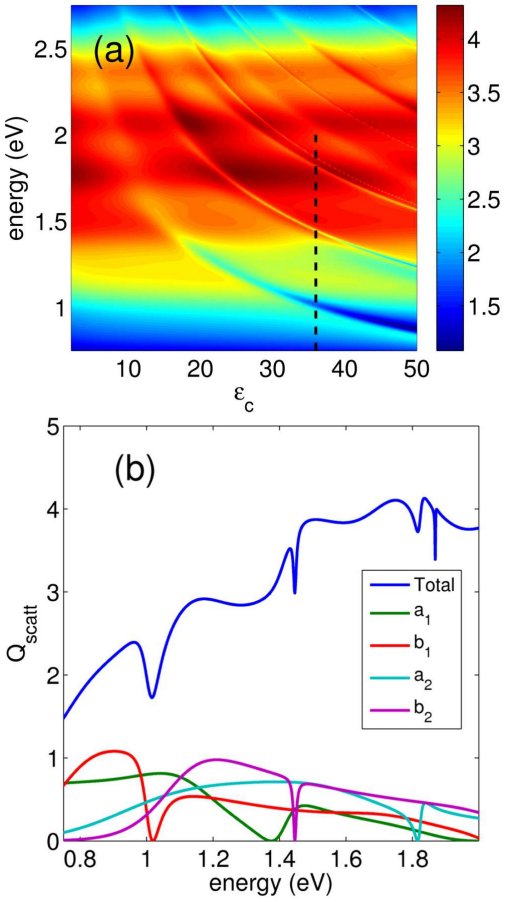

Figure 4 Scattering efficiency of a dielectric-core silica-shell particle with r_c = 100 nm and r_s = 500 nm as function of the photon energy and core dielectric function (a). The scattering efficiency for the case of $\varepsilon_c = 36$ is shown in (b), together with the partial contributions from different multipolar orders.

3.2 Illumination conditions

A common feature to all FR in the core-shell systems described above is that the contribution from multipoles of different order than the FR add incoherently to the total scattering and affect the overall line-shape. However, control on the excitation of

different multipolar orders can be addressed by adjusting the illumination conditions. It has been shown that higher order resonances can be quenched by using strongly focused beams, both in single particles[41] and particle clusters[39]. We can consider the effect of focused plane waves by the extension of the generalized Mie theory described in Section 2. In this way we can analyze the influence of the focusing degree on the excitation of FR. The simulation scheme considers a plane wave arriving to an aplanatic lens that is characterized by a semi-aperture angle α (Fig. 5.a). The particle is placed at the focus of the lens. One should note that normalized efficiences (see Section 2) are used here in order to enable comparison with plane wave excitation. Figure 5.b shows the influence of α on the normalized scattering efficiency of a dielectric-core silver-shell particle with $\varepsilon_c = 9$, $r_c = 15$ nm and $r_s = 65$ nm. The dipolar cavity-like mode is excited at 2.94 eV while the sphere-like quadrupolar mode is closely located at 3 eV. By increasing the degree of focusing, the quadrupolar resonance is quenched and an enhanced Fano line-shape in the scattering spectra can be observed. The influence of the excitation characteristics is also evidenced in the near field distribution at the photon energy corresponding to the Fano dip of the scattering spectra. For a plane wave excitation (Fig. 5.c) the near field distribution shows a typical quadrupole signature, while for a strongly focused plane wave (Fig. 5.d) the incomplete cancellation of the dipole moments associated with the cavity-like and sphere-like modes results in dipolar-like characteristics. These observations are supported also by the calculation of the far-field radiation patterns that show a combination of quadrupolar and dipolar characteristics for a plane wave excitation (Fig 5.e) and only dipolar lobes for tight focusing (Fig 5.f).

Alternatively, low order multipolar resonances can be quenched if the excitation beam is properly polarized. Thus, Hermite-Gaussian and Laguerre-Gaussian beams are able to inhibit the formation of a hot-spot at the gap between rod antennas associated with the coupled dipolar mode excitation[70]. Figure 6 shows the normalized extinction, scattering and absorption efficiencies when a lens with semi-aperture of 90° is illuminated by a plane wave or by an $x-$polarized Hermite-Gaussian beam of order 0 and degree 1. In the first case the higher order quadrupolar mode is quenched, while in the second case the dipolar resonance is not excited and the scattering spectrum is dominated by the quadrupolar FR. One has to take into account that in order to quench the dipolar resonance the phase jump in the light distribution exciting the particle has to be in a direction perpendicular to the polarization. Otherwise a longitudinal component of the field appears[71] that leads to the excitation of dipolar bright modes[44].

Regarding the effect of the polarization distribution on the optical response of nanostructures, it has to be mentioned the unique potential of cylindrical vector beams[72] to control plasmonic resonances . It is the case of excitation of ring modes

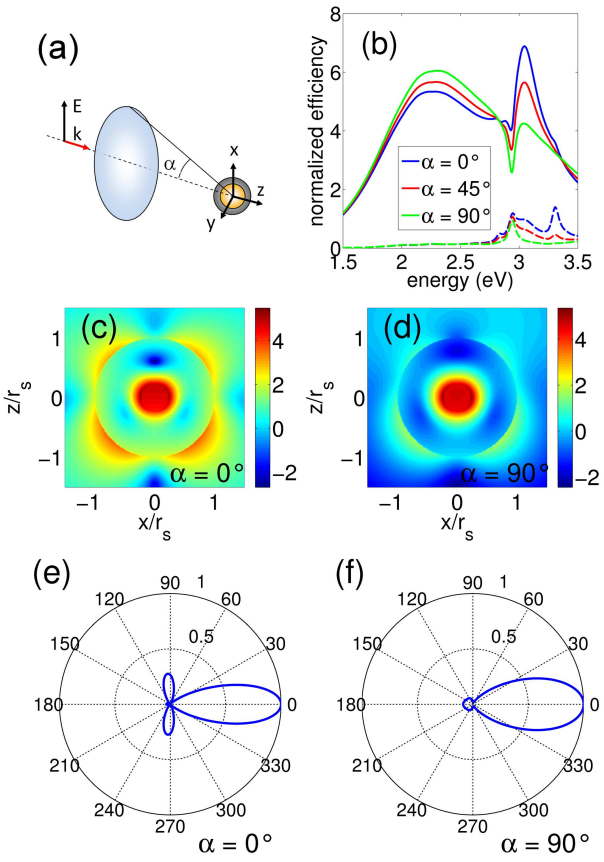

Figure 5 a) Excitation of a core-shell with a focused plane wave (FPW). b) Normalized scattering (solid) and absorption (dash) efficiencies for a core with ε_c= 9 and silver shell with r_c = 15 nm and r_s = 65 nm excited by a FPW with different semi-apertures. c) and d) show the near field distribution of the square electric field amplitude (log scale) and e) and f) the normalized radiation patterns in the XZ plane.

in plasmonic clusters[44] that has been experimentally demonstrated in recent works[73,74]. In the context of FR in core-shell systems, one can take profit that a radially polarized (RP) beam is able to excite only electric multipolar modes[43] and inhibit magnetic modes. Figure 7.a shows the efficiencies of a silver-core silicon-shell particle with r_c = 68 nm and r_s = 225 nm surrounded by air. This particle configuration has been recently proposed as a structure able to achieve broadband unidirectional scattering response thanks to the combination of the electric dipole moment from the silver core and the magnetic dipole moment of the silicon shell that are excited in the same spectral region[75]. This characteristic is illustrated in the radiation pattern at the resonance peak (Fig 7.c). A close analysis shows that the electric dipolar contribution has an asymmetric line-shape characteristic of FR that results from the excitation of core plasmon mode and the electric dipolar contribution of the

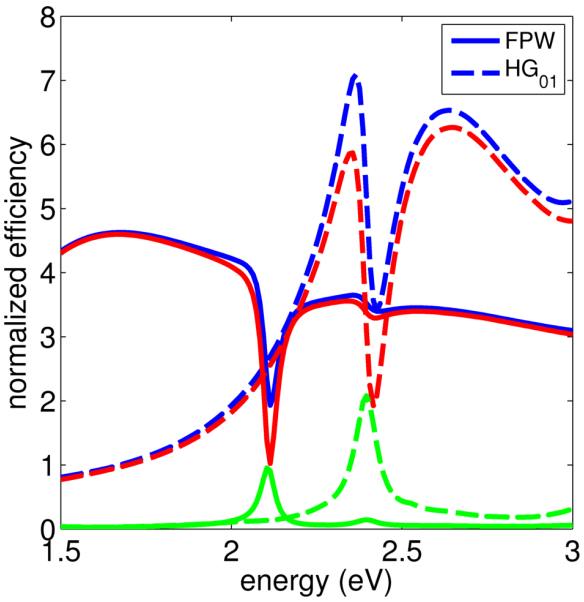

Figure 6 Normalized extinction (blue), scattering (red) and absorption (green) efficiencies of a dielectric-core silver-shell particle with $\varepsilon_c = 9$, $r_c = 50$ nm and $r_s = 100$ nm. The particle is located at the focus of a lens with semi-aperture $\alpha = 90°$ illuminated by a plane wave (solid) and by an x-polarized (0,1) Hermite-Gaussian beam.

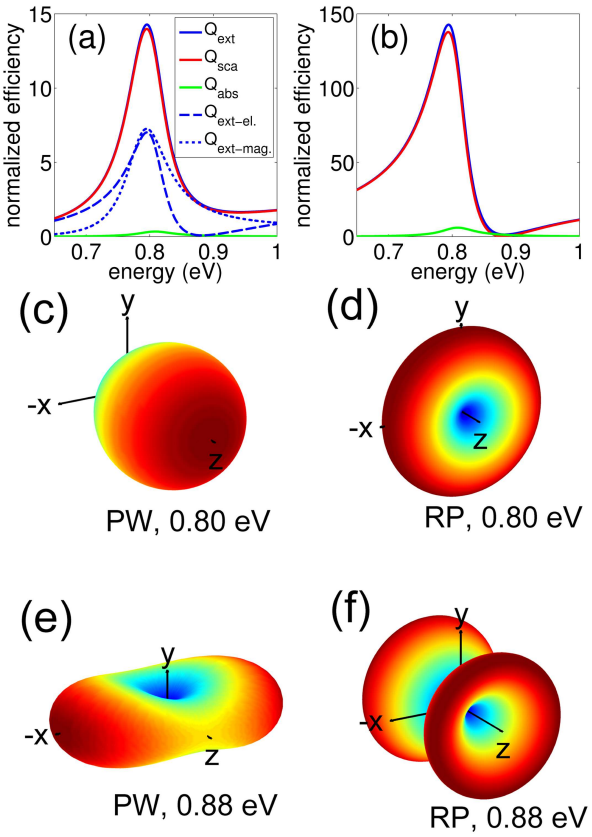

Figure 7 Extinction, scattering and absorption efficiencies of a silver-core silicon-shell ($\varepsilon_s = 11.56$) particle with $r_c = 68$ nm and $r_s = 225$ nm excited by a plane wave (PW) (a) and a focused radially polarized beam (RP) with $\alpha = 90°$ (b). Note that the normalized efficiency values are very large because the incident power crossing the particle vanishes on the z axis[43]. Radiation patterns at the maximum extinction efficiency (c, d) and at the Fano dip of the electric dipole (e, f)

silicon shell, in a similar fashion as discussed above (see Figure 4). Thus, at the wavelength where the Fano dip of the electric dipole resonance takes place and the electric dipolar contribution is minimized, the radiation pattern can be associated with the magnetic dipole oriented in the y-direction, i.e., excited by the plane wave magnetic field (Fig.7.e). If a strongly focused RP beam is used as excitation, the magnetic contributions are removed and only the electric modes can be excited (Fig. 7.b). At the scattering maximum the radiation pattern losses its unidirectional character and resembles the one of an electric dipole oriented in the z-direction, i.e., excited by the longitudinal component of the focused RP beam (Fig. 7.d). At the wavelength where the Fano dip takes place, the radiation pattern acquires the characteristics of an electric quadrupole (Fig. 7.f).

Complementing the previous case, inhibition of electric multipoles and exclusive excitation of magnetic modes can be achieved by using an azimuthally polarized (AP) beam. In Figure 8.a, the scattering properties of a silicon-core silver-shell particle illuminated by a plane wave show several Fano resonances of different multipolar orders. When the particle is located at the focus of a lens illuminated by an AP beam, only the dipolar magnetic response and, hence, its associated FR can be excited (Fig 8.b). By removal of the electric dipole contributions, the FR is significantly enhanced. Thus, while the ratio between scattering efficiencies at the peak and dip frequencies of the magnetic FR is 1.22 for plane wave excitation, a value of 4.26 is obtained when using an AP beam. The removal of the electric contribution also enables to get a closer insight on the characteristic field distribution of a dipolar magnetic FR. Thus, for energies below the FR (Fig. 8.c) the particle response at the focal plane is characterized by an electric field distribution indicating ring-shaped displacement currents that are parallel in the core and in the shell, i.e., by parallel dipolar magnetic moments in the perpendicular (z) direction. For energies above the FR (Fig. 8.d), the electric field lines show approximately opposite displacement currents in the shell and in the particle, i.e., the associated dipole magnetic moments in the perpendicular direction are anti-parallel.

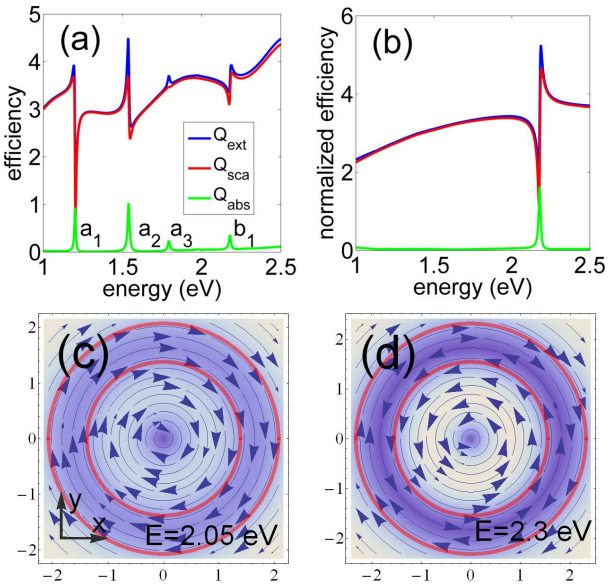

Figure 8 Extinction, scattering and absorption efficiencies of a core-shell particle with a core with ε_c= 11.56 and silver shell with r_c = 100 nm and r_s = 155 nm excited by a plane wave (a) and a focused azimuthally polarized beam with $\alpha = 90^\circ$ (b). Electric field circulation at the focal plane for energies below (c) and above (d) the magnetic Fano resonance

4 Conclusions

In summary, it has been shown that concentric single layer core-shell particles present inherent FR resulting from the interaction between cavity-like and sphere-like modes. Efficient excitation of these FR requires weak hybridization and the use of dielectric materials with large dielectric function in order to enhance the spectral overlapping between resonances. The involved modes do not have to be necessarily of plasmonic character, as FR can be obtained in all-dielectric core-shell particles using Mie resonances. Retardation can improve the FR strength and induced additional multipolar resonances. Enhancement of FR can be achieved by tailoring the illumination conditions in order to quench the excitation of unwanted modes that contribute incoherently to the scattering. Control of the illumination polarization and intensity distribution can dramatically modify the near field and far-field response of the particle for photon energies around the FR. Overall, it has been shown that a proper choice of material, sizes and illumination conditions may enable core-shell particles to become an effective nanostructure for the excitation of plasmonic FR.

Acknowledgements

The authors thank support of the Spanish Ministry of Economy and Competitivity through the project FIS2012-38244-C02-02.

Supplementary Information

Fits of the scattering spectra of core-shell particles to the electromagnetic model for Fano resonances proposed by Gallinet and Martin[54] and efficiency spectra for particles having a gold shell are provided in the Electronic Supplementary Information.

References

[1] A. E. Miroshnichenko, S. Flach and Y. S. Kivshar, *Reviews of Modern Physics*, 2010, **82**, 2257.

[2] B. Luk'yanchuk, N. I. Zheludev, S. A. Maier, N. J. Halas, P. Nordlander, H. Giessen and C. T. Chong, *Nature Materials*, 2010, **9**, 707–715.

[3] M. Rahmani, B. Luk'yanchuk and M. Hong, *Laser and Photonics Reviews*, 2013, **7**, 329–349.

[4] V. Giannini, Y. Francescato, H. Amrania, C. C. Phillips and S. A. Maier, *Nano Letters*, 2011, **11**, 2835–2840.

[5] A. Lovera, B. Gallinet, P. Nordlander and O. J. Martin, *ACS Nano*, 2013, **7**, 4527–4536.

[6] B. Hopkins, A. N. Poddubny, A. E. Miroshnichenko and Y. S. Kivshar, *Phys. Rev. A*, 2013, **88**, 053819.

[7] B. Gallinet, T. Siegfried, H. Sigg, P. Nordlander and O. J. F. Martin, *Nano Letters*, 2013, **13**, 497–503.

[8] N. Liu, M. Hentschel, T. Weiss, A. P. Alivisatos and H. Giessen, *Science*, 2011, **332**, 1407–1410.

[9] J. Ye, F. Wen, H. Sobhani, J. B. Lassiter, P. V. Dorpe, P. Nordlander and N. J. Halas, *Nano Letters*, 2012, **12**, 1660–1667.

[10] B. Gallinet and O. J. F. Martin, *ACS Nano*, 2013, **7**, 6978–6987.

[11] F. Hao, Y. Sonnefraud, P. V. Dorpe, S. A. Maier, N. J. Halas and P. Nordlander, *Nano Letters*, 2008, **8**, 3983–3988.

[12] P.-Y. Chen, J. Soric and A. Alù, *Advanced Materials*, 2012, **24**, OP281–OP304.

[13] C. Ayala-Orozco, J. G. Liu, M. W. Knight, Y. Wang, J. K. Day, P. Nordlander and N. J. Halas, *Nano Letters*, 2014, **14**, 2926–2933.

[14] W.-S. Chang, J. B. Lassiter, P. Swanglap, H. Sobhani, S. Khatua, P. Nordlander, N. J. Halas and S. Link, *Nano Letters*, 2012, **12**, 4977–4982.

[15] Z. Li, S. Zhang, L. Tong, P. Wang, B. Dong and H. Xu, *ACS Nano*, 2014, **8**, 701–708.

[16] J. B. Lassiter, H. Sobhani, J. A. Fan, J. Kundu, F. Capasso, P. Nordlander and N. J. Halas, *Nano Letters*, 2010, **10**, 3184–3189.

[17] J. B. Lassiter, H. Sobhani, M. W. Knight, W. S. Mielczarek, P. Nordlander and N. J. Halas, *Nano Letters*, 2012, **12**, 1058–1062.

[18] M. Rahmani, D. Y. Lei, V. Giannini, B. Lukiyanchuk, M. Ranjbar, T. Y. F. Liew, M. Hong and S. A. Maier, *Nano Letters*, 2012, **12**, 2101–2106.

[19] M. Hentschel, D. Dregely, R. Vogelgesang, H. Giessen and N. Liu, *ACS Nano*, 2011, **5**, 2042–2050.

[20] N. A. Mirin, K. Bao and P. Nordlander, *The Journal of Physical Chemistry A*, 2009, **113**, 4028–4034.

[21] M. Rahmani, E. Yoxall, B. Hopkins, Y. Sonnefraud, Y. Kivshar, M. Hong, C. Phillips, S. A. Maier and A. E. Miroshnichenko, *ACS Nano*, 2013, **7**, 11138–11146.

[22] B. Hopkins, W. Liu, A. E. Miroshnichenko and Y. S. Kivshar, *Nanoscale*, 2013, **5**, 6395–6403.

[23] M. Kerker, *J. Opt. Soc. Am.*, 1975, **65**, 376–379.

[24] S. Mukherjee, H. Sobhani, J. B. Lassiter, R. Bardhan, P. Nordlander and N. J. Halas, *Nano Letters*, 2010, **10**, 2694–2701.

[25] D. Wu, S. Jiang and X. Liu, *The Journal of Physical Chemistry C*, 2011, **115**, 23797–23801.

[26] O. Peña-Rodríguez, A. Rivera, M. Campoy-Quiles and U. Pal, *Nanoscale*, 2013, **5**, 209–216.

[27] J. F. Ho, B. Lukyanchuk and J. B. Zhang, *Applied Physics A*, 2012, **107**, 133–137.

[28] J. Zhang and A. Zayats, *Optics Express*, 2013, **21**, 8426–8436.

[29] J.-W. Liaw, H.-C. Chen and M.-K. Kuo, *Nanoscale Research Letters*, 2013, **8**, 1–8.

[30] P. Nordlander, *ACS Nano*, 2009, **3**, 488–492.

[31] O. Peña-Rodríguez and U. Pal, *Nanoscale*, 2011, **3**, 3609–3612.

[32] O. Peña-Rodríguez, U. Pal, M. Campoy-Quiles, L. Rodríguez-Fernández, M. Garriga and M. Alonso, *The Journal of Physical Chemistry C*, 2011, **115**, 6410–6414.

[33] H. Chen, L. Shao, Y. C. Man, C. Zhao, J. Wang and B. Yang, *Small*, 2012, **8**, 1503–1509.

[34] T. J. Arruda, A. S. Martinez and F. A. Pinheiro, *Phys. Rev. A*, 2013, **87**, 043841.

[35] F. Monticone, C. Argyropoulos and A. Alù, *Scientific Reports*, 2012, **2**, 912.

[36] H. L. Chen and L. Gao, *Opt. Express*, 2013, **21**, 23619–23630.

[37] C. F. Bohren and D. R. Huffman, *Absorption and Scattering of Light by Small Particles*, Wiley. com, 2008.

[38] A. L. Aden and M. Kerker, *Journal of Applied Physics*, 1951, **22**, year.

[39] J. Sancho-Parramon, *Optics Letters*, 2011, **36**, 3527–3529.

[40] C. Sheppard and P. Török, *Journal of Modern Optics*, 1997, **44**, 803–818.

[41] N. M. Mojarad, V. Sandoghdar and M. Agio, *J. Opt. Soc. Am. B*, 2008, **25**, 651–658.

[42] R. Borghi, M. Santarsiero and M. A. Alonso, *J. Opt. Soc. Am. A*, 2005, **22**, 1420–1431.

[43] N. M. Mojarad and M. Agio, *Optics Express*, 2009, **17**, 117–122.

[44] J. Sancho-Parramon and S. Bosch, *ACS Nano*, 2012, **6**, 8415–8423.

[45] O. Peña, U. Pal, L. Rodríguez-Fernández and A. Crespo-Sosa, *J. Opt. Soc. Am. B*, 2008, **25**, 1371–1379.

[46] R. D. Averitt, S. L. Westcott and N. J. Halas, *J. Opt. Soc. Am. B*, 1999, **16**, 1824–1832.

[47] R. Bardhan, N. K. Grady, T. Ali and N. J. Halas, *ACS Nano*, 2010, **4**, 6169–6179.

[48] C. S. Levin, C. Hofmann, T. A. Ali, A. T. Kelly, E. Morosan, P. Nordlander, K. H. Whitmire and N. J. Halas, *ACS Nano*, 2009, **3**, 1379–1388.

[49] E. Prodan, C. Radloff, N. Halas and P. Nordlander, *Science*, 2003, **302**, 419–422.

[50] S. A. Maier, *Plasmonics: Fundamentals and Applications*, Springer, 2007.

[51] N. J. Halas, S. Lal, W.-S. Chang, S. Link and P. Nordlander, *Chemical Reviews*, 2011, **111**, 3913–3961.

[52] N. E. Rehler and J. H. Eberly, *Phys. Rev. A*, 1971, **3**, 1735–1751.

[53] P. B. Johnson and R.-W. Christy, *Physical Review B*, 1972, **6**, 4370.

[54] B. Gallinet and O. J. Martin, *Physical Review B*, 2011, **83**, 235427.

[55] B. Gallinet and O. J. Martin, *ACS Nano*, 2011, **5**, 8999–9008.

[56] N. Verellen, Y. Sonnefraud, H. Sobhani, F. Hao, V. V. Moshchalkov, P. V. Dorpe, P. Nordlander and S. A. Maier, *Nano Letters*, 2009, **9**, 1663–1667.

[57] C. Sönnichsen, T. Franzl, T. Wilk, G. von Plessen, J. Feldmann, O. Wilson and P. Mulvaney, *Physical Review Letters*, 2002, **88**, 077402.

[58] T. Teperik, V. Popov and F. G. de Abajo, *Physical Review B*, 2004, **69**, 155402.

[59] C. W. Hsu, B. G. DeLacy, S. G. Johnson, J. D. Joannopoulos and M. Soljai, *Nano Letters*, 2014, **14**, 2783–2788.

[60] K. Laaksonen, S. Suomela, S. R. Puisto, N. K. J. Rostedt, T. Ala-Nissila and R. M. Nieminen, *J. Opt. Soc. Am. B*, 2014, **31**, 494–502.

[61] A. E. Miroshnichenko, *Physical Review A*, 2010, **81**, 053818.

[62] F. Monticone, C. Argyropoulos and A. Alù, *Phys. Rev. Lett.*, 2013, **110**, 113901.

[63] A. I. Kuznetsov, A. E. Miroshnichenko, Y. H. Fu, J. Zhang and B. Lukyanchuk, *Scientific Reports*, 2012, **2**, 492.

[64] N. T. Fofang, T.-H. Park, O. Neumann, N. A. Mirin, P. Nordlander and N. J. Halas, *Nano Letters*, 2008, **8**, 3481–3487.

[65] A. García-Etxarri, R. Gómez-Medina, L. S. Froufe-Pérez, C. López, L. Chantada, F. Scheffold, J. Aizpurua, M. Nieto-Vesperinas and J. Sáenz, *Optics Express*, 2011, **19**, 4815–4826.

[66] A. E. Miroshnichenko and Y. S. Kivshar, *Nano Letters*, 2012, **12**, 6459–6463.

[67] K. E. Chong, B. Hopkins, I. Staude, A. E. Miroshnichenko, J. Dominguez, M. Decker, D. N. Neshev, I. Brener and Y. S. Kivshar, *Small*, 2014, **10**, 1985–1990.

[68] A. Moroz, *The Journal of Physical Chemistry C*, 2009, **113**, 21604–21610.

[69] S. N. Sheikholeslami, H. Alaeian, A. L. Koh and J. A. Dionne, *Nano Letters*, 2013, **13**, 4137–4141.

[70] G. Volpe, S. Cherukulappurath, R. Juanola Parramon, G. Molina-Terriza and R. Quidant, *Nano Letters*, 2009, **9**, 3608–3611.

[71] L. Novotny and B. Hecht, *Principles of Nano-optics*, Cambridge University Press, 2012.

[72] Q. Zhan, *Advances in Optics and Photonics*, 2009, **1**, 1–57.

[73] D. Gómez, Z.-Q. Teo, M. Altissimo, T. J. Davis, S. Earl and A. Roberts, *Nano Letters*, 2013, **13**, 3722–3728.

[74] A. Yanai, M. Grajower, G. M. Lerman, M. Hentschel, H. Giessen and U. Levy, *ACS Nano*, 2014, **8**, 4969–4974.

[75] W. Liu, A. E. Miroshnichenko, D. N. Neshev and Y. S. Kivshar, *ACS Nano*, 2012, **6**, 5489–5497.